A study of the slope probability density function of the ocean waves from radar observations

D. Hauser,[1,2] G. Caudal,[1,2] S. Guimbard,[3] and A. A. Mouche[3,4]

[1] Radar observations of the sea surface at C-Band and small incidence angles are used to investigate some properties of the surface slope probability density function (pdf). The method is based on the analysis of the variation of the radar cross-section with incidence angle, assuming a backscattering process following the Geometrical Optics theory. First, we assess the limit of this model in our experimental configuration by using simulations of radar cross-sections with a more accurate backscattering model, namely the Physical Optics model. We show that roughness properties with scales larger than 12 cm can be analyzed in our configuration (C-Band, incidence 7 to 16°). The radar data are then analyzed in terms of filtered mean square slope under the assumption of a Gaussian slope pdf. Dependence of the radar-derived mean square slopes (mss) with wind speed is analyzed, thanks to wind estimates obtained by using coincident observations of the same radar at larger incidence (around 32°). Furthermore an analysis of the anisotropy of the mean square slope is proposed. The results are discussed in comparison with those of Cox and Munk (1954a, 1954b), and with the mean square slopes derived from two surface models (Elfouhaily et al., 1997 and Kudryavtsev et al., 2003). We find that the radar-derived values are in good agreement with Cox and Munk results, taking into account the filtering effect on radar-derived values. We also show that the surface model of Elfouhaily et al. yields good agreement for the omni directional mss, but a too large anisotropy of the mss. The model of Kudryavtsev provides a reasonable anisotropy of the mss, but overestimates the mss values in all directions. Finally, we propose an analysis of the radar data under a non-Gaussian assumption for the slope pdf, by applying the compound model suggested by Chapron et al. (2000) to our observations. To our knowledge, it is the first time that peakedness values are explicitly derived from radar observations, and documented as a function of azimuth and wind speed. We show that the peakedness (or kurtosis) of the slope pdf is not zero but weak (peakedness factor reaching about 0.20), and slightly increases with wind speed.

1. Introduction

[2] It is well known that the normalized radar cross-section of the ocean surface at small incidence can be assumed to be proportional to the probability density function (pdf) of surface wave slopes, thanks to the Geometric Optics approximation proposed by *Barrick* [1968a], which represents the quasi-specular reflection from ocean facets. The slope pdf is usually regarded as Gaussian, with a variance (called mean square slope or mss), mainly governed by the short wind waves and increasing with wind speed [*Cox and Munk*, 1954a, 1954b]. On the basis of these

results, the normalized radar cross-section measured by radar altimeters can be related analytically to the mean square slope of waves, which in turn is a function of wind speed. In practice however, empirical relationships [e.g., *Witter and Chelton*, 1991; *Freilich and Challenor*, 1994] are used to infer wind speed from the normalized radar cross-section at nadir.

[3] Indeed, it still remains difficult to use physically based models for such inversion [*Chelton et al.*, 2001]. The main reason is that the range of waves which contribute to the backscatter modeled under the Geometrical Optics approximation is not well determined and depends at least on radar frequency and incidence angle [see *Thompson et al.*, 2005]. The Geometric Optics approximation is only valid for the high frequency limit (microwave wavelength much smaller than the radius of curvature of the scattering surface), which means, as shown by *Thompson et al.* [2005], that it tends to filter out the properties of the waves shorter than a certain limit. The second difficulty in invert-

[1]Université de Versailles Saint-Quentin, CETEP-IPSL, Vélizy, France.
[2]CNRS, CETP-IPSL, Vélizy, France.
[3]IFREMER, Brest, France.
[4]Now at Boost-Technologies, Brest, France.

ing the radar signal at small incidence by using the Geometrical Optics model is the shortwave diffraction effect, which also filters out the shortest waves [see also *Thompson et al.*, 2005, or *Jackson et al.*, 1992]. Because of both effects (artificial cutoff or diffraction effects) radar observations at small incidence angle can only be used to estimate an "effective" mean square slope. The relation between this effective (or filtered) mean square slope and the true mean square slope is not well known, in particular because the shape of the wave slope spectrum is not well known in the domain filtered by the radar (gravity-capillary and short gravity waves).

[4] Several questions therefore remain open regarding the interpretation of the radar backscatter at small incidence in terms of surface mean square slope. First, as mentioned above, the filtering effect in radar measurements needs to be better estimated. This is required to infer statistical properties of the surface from radar observations, and to compare these properties with those given by other empirical methods (from surface spectra observations, optical measurements, etc). This is also necessary to develop models for the estimation of surface parameters from multistatic observations as provided by Global Positioning Systems. Secondly, although it is admitted that the slope pdf can be considered as Gaussian at the first order [*Cox and Munk*, 1954a, 1954b], it is also recognized that the short waves exhibit non-Gaussian properties [*Cox and Munk*, 1954a, 1954b; *Longuet-Higgins*, 1963; *Longuet-Higgins*, 1982; *Shaw and Churnside*, 1997].

[5] Few measurements have been carried out in the past to document the slope pdf. Most of them rely on indirect observations of the sea scatter either from optical techniques [*Cox and Munk*, 1954a, 1954b; *Shaw and Churnside*, 1997] or microwave techniques [*Jackson et al.*, 1992]. *Vandemark et al.* [2004] proposed slope pdf estimates by using range measurements with an airborne laser, but the approach provides information only in a non-directional sense, and for waves longer than about 2 m in wavelength. *Hwang and Wang* [2004] and *Hwang* [2005] made in situ spectral measurements of ocean waves from a free-drifting buoy to avoid artifacts due to Doppler effects. However, their measurements concern waves shorter than about 6 m in wavelength, so that for estimating the variance of the slope pdf, some assumptions about longer waves are required. They do not provide information on cumulants (or moments) of the slope pdf other than the mean square slope. This short review shows that we still have to rely on indirect observations, and in particular on microwave observations to further improve our knowledge of the slope pdf and of its cumulants. *Jackson et al.* [1992] proposed a theoretical analysis based on electromagnetic modeling, to relate the effective mean square slope estimated from microwave observations under various conditions, and given a prescribed wave height spectrum. *Thompson et al.* [2005] proposed an objective method to estimate the filter limit in wave number associated with the microwave methods. *Chapron et al.* [2000] proposed a method to estimate from microwave observations, the 4th order cumulant of the slope pdf (i.e., the kurtosis or peakedness parameter), in addition to the second cumulant (or mean square slope).

[6] The aim of the present study is first to improve our knowledge of the filtered mean square slope derived from radar observations under Gaussian assumptions. Observations performed with an airborne radar at C-Band (5.35 GHz) are used to investigate the dependence of the effective (or filtered) mean square slope of the waves with wind speed, and its angular dependence with azimuth. The range of wave numbers, which contribute to this effective mean square slope, is first established. Our results are then compared with those of *Cox and Munk* [1954a, 1954b] and with mean square slopes given by classical wave spectra of the literature, namely the *Elfouhaily et al.* [1997] spectrum, and the *Kudryavtsev et al.* [2003] spectrum- hereafter referred to as ECKV and KHCC spectra, respectively. This comparison allows us to point out some drawbacks of these empirical spectra, concerning either their ability to reproduce the filtered mss (KHCC) or the anisotropy of the mss (ECKV).

[7] In a second step, the same data set is used to investigate a possible deviation from a Gaussian shape of the slope pdf. For that purpose, we analyze our data set by using the concept of "compound model" proposed by *Chapron et al.* [2000]. The results are analyzed for a large range of wind speeds and in all azimuth directions with respect to the wind direction.

[8] The paper is organized as follows. In section 2, we briefly describe the experimental conditions. Section 3 explains the methodology of the data analysis: interpretation of profiles of radar cross-section with incidence (at small incidence) in terms of mean square slope under a Gaussian assumption, discussion on filtering effects, analysis of non-Gaussian effects, estimation of wind speed from radar cross-section at moderate incidence. Section 4 presents the results: mean square slope as a function of wind speed under Gaussian assumption, anisotropy of the mean square slope (Gaussian assumption), non-Gaussian effects. Finally we conclude in section 5.

2. Experimental Conditions

[9] The data set comes from observations performed with the airborne radar called STORM [see, e.g., *Mouche et al.*, 2005]. STORM is a real aperture radar operating in C-Band (5.35 GHz) mounted on aircraft and used for specific research campaigns. It is a multipolarization radar, but here we have used only VV-polarized data. It uses a large beam antenna (two-way beam aperture $30 \times 7.6°$), pointing at a mean incidence angle of $20°$, and scanning in azimuth at a rate of 2 rotations per minute. It has a 1.5 m resolution in range, allowing an analysis of the observations versus incidence angle with a good accuracy. The data are processed to provide profiles of radar cross-section as a function of incidence angle every $1°$ from about 7 to $35°$, and as a function of azimuth directions every $0.4°$ over $360°$.

[10] STORM was used during the VALPARESO experiment [*Mouche et al.*, 2005] in the context of the calibration and validation exercise supported by ESA after the launch of ENVISAT. The experimental zone was off the Atlantic coasts of France. The meteo-oceanic buoy "Pharos" ($48°31'42''$N, $5°49'03''$W) was frequently over-flown by STORM. For the analysis presented below, we have used data from the 15 different flights performed in different sea surface conditions, each flight providing data along a

trajectory of several hundreds of kilometers in open sea conditions. The wind speeds as given by the Pharos buoy range from 4 to 16 m/s for this data set.

3. Methodology

3.1. Radar Filtered Mean Square Slope Under Gaussian Assumptions

[11] As first shown by *Barrick* [1968b] and then used in numerous works for analyzing radar observations at small incidence [see, e.g., *Jackson et al.*, 1985; *Jackson et al.*, 1992; *Hesany et al.*, 2000; *Freilich and Vanhoff*, 2003; *Vandemark et al.*, 2004; *Thompson et al.*, 2005; *Caudal et al.*, 2005], the normalized radar cross-section σ_0 at small incidence can be approximated by the Geometric Optics (GO) model which states that σ_0 is proportional to the probability density function (pdf) of the surface slopes:

$$\sigma_0(\theta) = |R(0)|^2 \pi \frac{p(\zeta_x, \zeta_y)}{\cos^4 \theta}, \tag{1}$$

where θ is the incidence angle, $R(0)$ is the Fresnel coefficient for normal incidence, $p(\zeta_x, \zeta_y)$ is the joint probability density function of slopes for surface waves longer than the diffraction limit, and evaluated at the specular points. ζ_x, ζ_y are the slope components of the rough surface in two orthogonal directions. The limit of diffraction, which depends on the electromagnetic wavelength, will be discussed below.

[12] If one further assumes that the slope pdf is Gaussian, with mean square slopes s_u^2 and s_c^2 in the upwind and crosswind directions respectively, σ_0 can be written as:

$$\sigma_0(\theta, \phi) = \frac{|R|^2}{\cos^4 \theta} \frac{1}{2s_u s_c} \exp\left(-\frac{\tan^2 \theta}{2}\left(\left(\frac{\cos\phi}{s_u}\right)^2 + \left(\frac{\sin\phi}{s_c}\right)^2\right)\right), \tag{2}$$

where ϕ is the azimuth direction of the radar observation with respect to the wind direction.

[13] One can define the mean square slope s_ϕ^2 in the direction of observation ϕ, according to:

$$\frac{1}{s_\phi^2} = \frac{\cos^2 \phi}{s_u^2} + \frac{\sin^2 \phi}{s_c^2}, \tag{3}$$

and write (2) in the form:

$$\sigma_0(\theta, \phi) = \frac{|R|^2}{\cos^4 \theta} \frac{1}{2s_u s_c} \exp\left(-\frac{\tan^2 \theta}{2s_\phi^2}\right), \tag{4}$$

or,

$$\ln\left(\sigma_0(\theta, \phi)\cos^4\theta\right) = \ln\left(\frac{|R|^2}{2s_u s_c}\right) - \frac{\tan^2 \theta}{2s_\phi^2}. \tag{5}$$

To estimate the mean square slope s_ϕ^2 in the ϕ direction, a fit of a linear function is applied to the radar observations of $\ln(\sigma_0(\theta, \phi)\cos^4\theta)$ expressed as a function of $(\tan^2\theta)$. The slope of the fitted linear function is inversely proportional to s_ϕ^2. The domain of incidence angles used for this fit is taken

between 7° and 16°. This range of incidence angles is chosen first because of the geometry of observations (very few observations at incidence smaller than 7°) and secondly to keep solutions with high quality of the fit (see section 3.2 below). In this incidence range, HH and VV are not significantly different, therefore the results are the same in HH and VV.

[14] This method provides a mean square slope that does not account for the smallest surface waves. Indeed, due to the diffraction process and to the Geometric Optics approximation [see *Thompson et al.*, 2005], the modeled radar backscatter is not sensitive to slopes of waves smaller than a certain limit. This limit is of the order of magnitude of several electromagnetic wavelengths, and the ratio depends at least on the electromagnetic wavelength, and on the range of incidence angles used in the analysis. This will be discussed in section 3.2. In the following the mean square slope estimated from the radar will be called "radar filtered mean square slope".

[15] The fit of equation (5) to the data is applied in each azimuth direction sampled by the radar, including the upwind and crosswind directions, which are determined from a separate analysis of the radar cross-section at larger incidence angles (see section 3.4).

[16] The total radar filtered mean square slope of the surface, s_t^2, can then be calculated as:

$$s_t^2 = s_u^2 + s_c^2, \tag{6}$$

and the omni-directional radar filtered mean square slope of the surface, s_o^2, is:

$$s_o^2 = \frac{s_u^2 + s_c^2}{2} = \frac{s_t^2}{2} \tag{7}$$

3.2. Minimum Wavelength Contributing to the Radar Filtered Mean Square Slope

[17] According to previous studies, the lower limit of wavelength contributing to the radar filtered mean square slope is two to ten times the electromagnetic wavelength [see, e.g., *Jackson et al.*, 1992]. For a C-band radar this means between 10 cm and 50 cm. This is a range where the mean square slope, when calculated from the integral of the spectral density of wave slopes, is sensitive to the upper limit of integration in wave number [*Caudal*, 1993]. Therefore it is important to estimate the exact range of wavelengths that contributes to the radar filtered mean square slope.

[18] To do this, we have followed the method proposed by *Thompson et al.* [2005]. First, we model the radar cross-section using the Physical Optics model, hereafter referred to as PO model (or Kirchhoff model), which has a broader range of applicability than the GO model (see Appendix A). The expression of the Kirchhoff model given in Appendix A, was derived by assuming Gaussian statistics of the surface elevation. The method is similar to that originally proposed by *Jackson et al.* [1992], and also used in a bistatic configuration by *Thompson et al.* [2005]. We consider a surface description given by the two-dimensional spectrum from either ECKV or KHCC (see Appendix B).
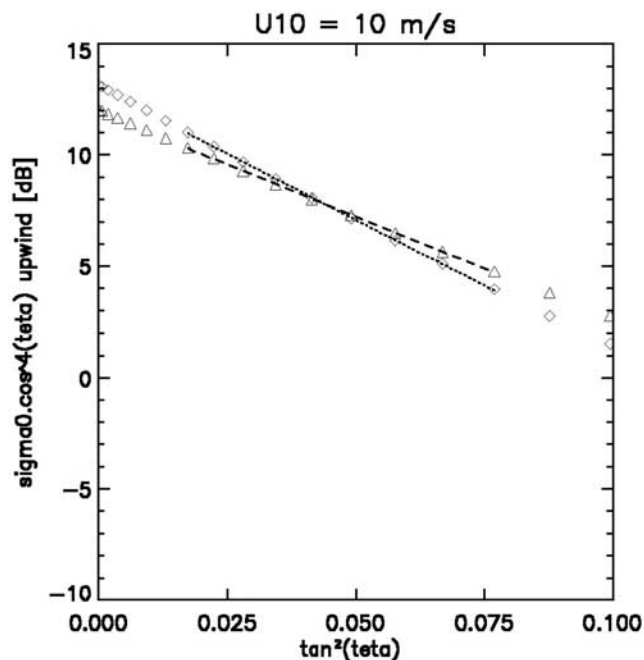
Figure 1. $\sigma_0(\theta, \phi)\cos^4\theta$ (in dB) as a function of $\tan^2\theta$, as simulated by the Physical Optics model (see appendix A) and the sea surface spectrum given for a 10 m/s wind speed, by *Elfouhaily et al.* [1997] (diamonds) and *Kudryavtsev et al.* [2003] (triangles). The solid and dashed lines are the fit of equation (5) to the model results, applied in the incidence range $[7-16°]$.

From the modeled values of σ_0, we estimate the radar fitted mean square slope as explained in section 3.1, by fitting equation (5) to the PO model results.

[19] Figure 1 shows the normalized radar cross-section as a function of the tangent square of incidence angle, simulated by using the Physical Optics model and the surface description of either ECKV (diamonds) or KHCC (triangles), for a 10 m/s wind speed. The dotted and dashed lines are the corresponding fits using equation (5). This figure clearly shows that the GO approximation is a good approximation in this range of incidence angle $(7-16°)$ with RMS difference between points and fit of about 0.04 dB and 0.02 dB for each case. Similar results are obtained in other directions of observations with respect to the wind direction, and for other wind speeds. The slope of the fitted lines is inversely proportional to the radar-filtered mean square slope (see equation (5)). Using this method, we investigated the impact of a change of the incidence angle range in the fit of equation (5). We found that the quality of the fit decreases significantly when the upper limit of incidence angles is increased (rms error of the fit increases to more than 0.1 dB when the range is increased to $[7-20°]$. The results also show that for wind speeds larger than 4 m/s, the radar-filtered mean square slopes derived from the $[7-16°]$ incidence range differs by less than 10% from the values derived in the range $[0-10°]$. When the incidence range is chosen as $[7-20°]$, this difference is larger than 15% for all wind speeds. This decrease of the quality of the fit when the upper limit of incidence angles is increased is due to the

change in backscatter mechanisms at larger incidence (more important curvature effects, Bragg scattering), which cannot be taken into account by a simple GO model. Therefore we consider in the following that using the incidence range $[7-16°]$ to fit equation (5) to experimental values is a good compromise.

[20] In order to estimate the maximum wave number k_d which contributes to the radar filtered mean square slope, we compare this latter with the mean square slope obtained from the integration of the surface wave spectrum used in the simulation. k_d is determined as being the upper limit of the integral, which gives the best agreement between the radar filtered mean square slope and the spectrum derived mean square slope.

[21] Figure 2 shows a scatterplot of the mean square slope from the surface spectrum, versus the mean square slope from the radar cross-section, for simulations performed with ECKV (Figure 2a) and with KHCC (Figure 2b) spectra, and for wind speed values between 2 and 20 m/s. The different symbols are for different values of k_d. The fit to the simulated radar cross-section has been applied here in the range of incidence angles $[7°-16°]$. Figure 2 shows that for both surface spectra, the best agreement between the two calculations of mean square slope is obtained for $k_d = 51$ rad/m (i.e., wavelength of 12.3 cm, which is 2.2 times the electromagnetic wavelength). It is important to note that a unique value of k_d is found for all mean square slope values larger than 0.025 (i.e., for all wind speeds higher than 4 m/s). This result is somewhat different from that of *Thompson et al.* [2005], who find a sensitivity of the cutoff wave number to wind speed, and significantly larger values of k_d. These differences can probably be explained by the smaller incidence angle range considered here $(7-16°)$ compared to that considered by *Thompson et al.* [2005]. Indeed, we could check that changing the range of incidence angles for estimating the filtered mean square slope not only changes the quality of the fit, but also the value obtained for k_d. The filtering not only depends on the electromagnetic wavelength as mentioned by previous authors [see, e.g., *Thompson et al.*, 2005], but also on the incidence range used to estimate the mean square slope. Variation with the prescribed surface wave spectrum (ECKV or KHCC) is less important although it still exists also. The value of k_d found here ($k_d = 51$ rad/m) is applicable for C-Band and the $[7-16°]$ range of incidence angle. In the following the mean square slopes derived from our radar observations in the range $[7-16°]$ will be compared to surface mean square slopes estimated from surface observations filtered at $k_d = 51$ rad/m.

3.3. Taking Into Account Non-Gaussian Statistics

[22] The analysis presented above is based on the assumption that the surface slopes exhibit Gaussian statistics. This is a correct approximation at the first order, although it is known since the work of *Cox and Munk* [1954a, 1954b] that differences from this Gaussian statistics do exist. *Chapron et al.* [2000] propose a parameterization of the slope pdf peakedness, which accounts from random variations of the slope variance between different patches of the sea surface considered as locally Gaussian. They show that this interpretation is consistent with both the analysis proposed by *Cox and Munk* [1956] of their sun glint observations [*Cox and Munk*, 1954a, 1954b], and with the
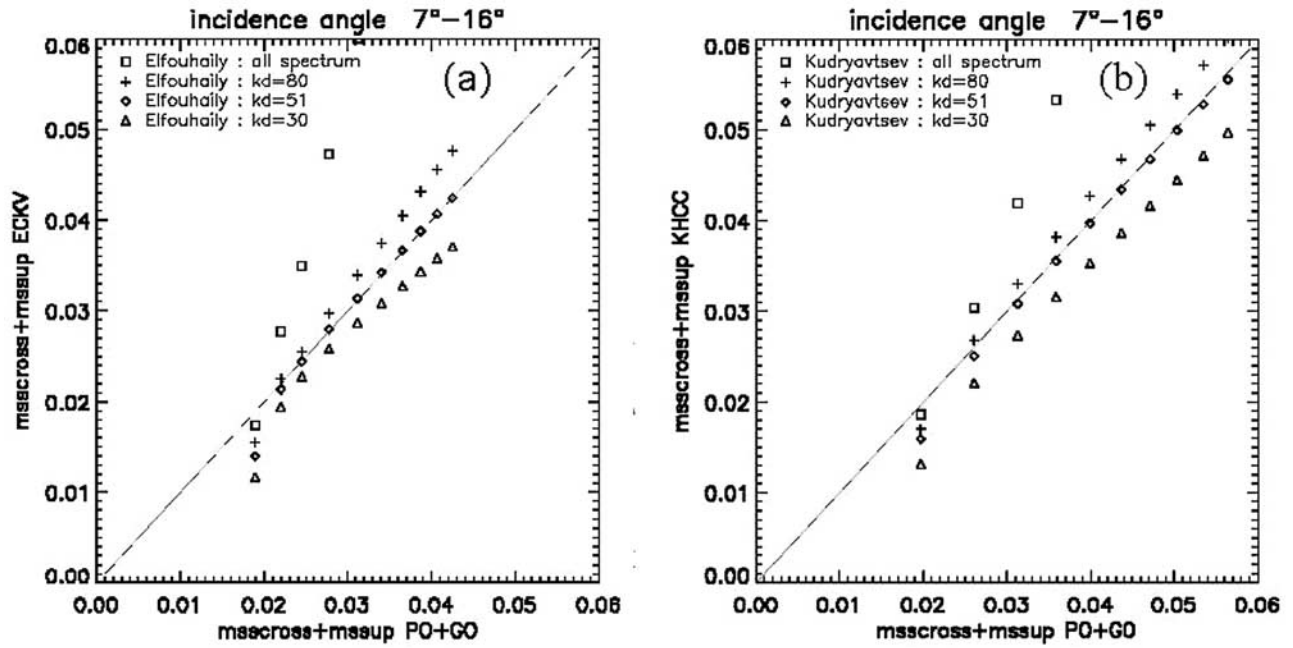
Figure 2. Total mean square slope (sum of upwind and crosswind values) estimated from the surface spectrum ((a) *Elfouhaily et al.* [1997], (b) *Kudryavtsev et al.* [2003]), as a function of the total mean square slope estimated from the fit to equation (5) on radar cross-section calculated with the Physical Optics model. The different symbols are for different values k_d of the wave number limit used in the integration for the surface spectrum.

analysis of the normalized radar cross-section at nadir as measured by satellite altimeters using the specular point (or Geometrical Optics) theory. We follow here the same approach, with an extension to the two-dimensional case.

[23] As proposed by *Chapron et al.* [2000], we assume that the local slope probability density function P, is Gaussian. In each direction of observation, it can be written as:

$$P\left(\eta_\phi\right) = \frac{1}{2\pi}\frac{1}{s_u s_c}\exp\left(-\frac{1}{2}\frac{\eta_\phi^2}{s_\phi^2}\right) \qquad (8)$$

where s_f^2 and η_ϕ are respectively the mean square and the local slope in the direction of observations.

[24] Following the compound model approach proposed by *Chapron et al.* [2000], we assume that the inverse α_ϕ of s_ϕ^2 ($\alpha_\phi = 1/s_\phi^2$) is a random variable, which can be expressed as:

$$\alpha_\phi = \alpha_{0\phi}(1+\delta), \qquad (9)$$

where δ represents the random fluctuation around the so-called "overall inverse mean square slope" $\alpha_{0\phi}$, and write the overall slope pdf $P'(\eta_\phi)$ as the average of the locally Gaussian pdfs:

$$P'\left(\eta_\phi\right) = \int P\left(\eta_\phi|\alpha_\phi(\delta)\right)P(\delta)d\delta.$$

As in the work of *Chapron et al.* [2000], δ is assumed to have a zero mean value ($\langle\delta\rangle = 0$), and a variance Δ ($\langle\delta^2\rangle = \Delta$). By identifying this approach to the Gram-Charlier expansion

proposed by *Cox and Munk* [1954a, 1954b], *Chapron et al.* [2000] have shown that Δ also characterizes the peakedness (i.e., kurtosis) of the slope pdf.

[25] Furthermore, following one of the possible assumptions proposed by *Chapron et al.* [2000], we assume that the third moment of δ ($\langle\delta^3\rangle$) is not null, but corresponds to the one given by a Gamma distribution. Assuming that $(1+\delta)$ is distributed as a Gamma distribution, with a mean value equal to 1 and a variance Δ (corresponding to $\langle\delta\rangle = 0$, $\langle\delta^2\rangle = \Delta$), the resulting third moment $\langle\delta^3\rangle$ is equal to $2\Delta^2$.

[26] With these hypotheses now applied in the 2D case by assuming that δ has the same statistical properties in all azimuth directions, it can be verified that the slope pdf in the direction of observation ϕ is:

$$P'\left(\eta_\phi\right) = \int P\left(\eta_\phi|\alpha_\phi(\delta)\right)P(\delta)d\delta$$
$$= \int \frac{\sqrt{\alpha_{0u}\alpha_{0c}}(1+\delta)}{2\pi}\exp\left(-\frac{\alpha_{0\phi}(1+\delta)\eta_\phi^2}{2}\right)P(\delta)d\delta, \qquad (10)$$

where α_{0u} and α_{0c} are the value of $\alpha_{0\phi}$ in the upwind and crosswind directions, respectively.

[27] By expanding the exponential term using properties of the moments of the δ distribution as described above, we obtain:

$$P'\left(\eta_\phi\right) \cong \frac{\sqrt{\alpha_{0u}\alpha_{0c}}}{2\pi}\exp\left(-\frac{\alpha_{0\phi}\eta_\phi^2}{2}\right)$$
$$\cdot\left[1 - \Delta\frac{\alpha_{0\phi}}{2}\eta_\phi^2 + \frac{\Delta(1+2\Delta)\alpha_{0\phi}^2\eta_\phi^4}{8}\right] \qquad (11)$$
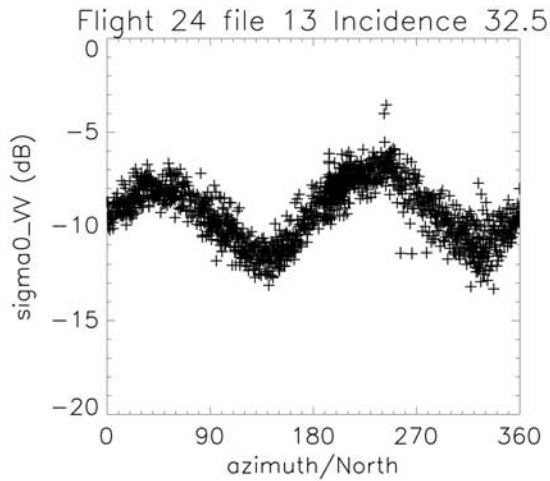
Figure 3. Example of STORM data: normalized radar cross-section in VV polarization at incidence 32.5 degrees, as a function of azimuth angle, obtained for a sample of 4 min of observations, in a case of strong wind (about 14 m/s).

Taking the logarithm of this expression and using an expansion up to the fourth power of surface slopes gives:

$$Ln\left(P'\left(\eta_\phi\right)\right) = A\eta_\phi^4 + B\eta_\phi^2 + C, \qquad (12a)$$

with

$$A = \frac{\alpha_{0\phi}^2 \Delta(1+\Delta)}{8}, \qquad (12b)$$

$$B = -\frac{\alpha_{0\phi}}{2}(1+\Delta), \qquad (12c)$$

$$C \propto \ln\left(\frac{\sqrt{\alpha_{0u}\alpha_{0c}}}{2\pi}\right). \qquad (12d)$$

The coefficients A, B, C are obtained from a quadratic fit applied to the radar observations expressed in logarithm units ($\ln(\sigma_0(\theta, \phi)\cos^4\theta)$) as a function of $\tan^2\theta = \eta_\phi^2$.

[28] The ratio $R = A/B^2$ is then used to derive the peakedness Δ:

$$R = \frac{A}{B^2} = \frac{\Delta}{2(1+\Delta)}, \qquad (13)$$

and the "overall mean square slope" is derived from equation (12c) or (12b).

[29] With the above assumptions, there is one and only one solution for Δ and $\alpha_{0\phi}$. In contrast, when the alternative assumption suggested by *Chapron et al.* [2000] is used (assuming $\langle\delta^3\rangle$ is null), equation (13) is replaced by a second order equation in Δ [see *Chapron et al.*, 2000], which may have either no solution or two solutions. We adopted therefore the assumption of $\langle\delta^3\rangle$ different from

zero, by choosing a Gamma distribution for the random variable $(1 + \delta)$.

[30] The same approach can also be used for a non-directional case. In that case, equations (12) are replaced by:

$$\ln(P(\eta)) \approx \ln\left(\frac{\alpha_0}{\pi}\right) - \alpha_0\eta^2(1+\Delta) + \frac{\Delta(1+\Delta)\alpha_0^2\eta^4}{2}, \qquad (14)$$

where the inverse of the omni-directional mean square slope α is:

$$\alpha = \alpha_0(1+\delta), \qquad (15)$$

and R has the same expression as in (13).

3.4. Wind Estimate

[31] Wind is estimated from the STORM observations at moderate incidence (32.5°) by using an empirical model of the classical form:

$$\sigma_0(\theta, \phi) = A_0[1 + A_1 \cos\phi + A_2 \cos(2\phi)], \qquad (16)$$

where A_0, A_1, A_2 are functions of incidence angle θ and wind speed (normalized as 10 m height wind speed in neutral atmospheric conditions).

[32] Figure 3 shows one example of STORM data as a function of azimuth angle (referred to the North), at incidence 32.5°. From a fit of equation (16) to these data, the upwind, downwind and crosswind directions are easily determined as corresponding to the maxima or minima of the fitted function.

[33] To estimate the wind speed, we chose the widely used empirical model CMOD2-I3 described by *Bentamy et al.* [1994]. We first compared winds inverted with CMOD2-I3 from STORM radar cross-sections, for samples close to the Pharos buoy (difference in time less than one hour, difference in space less than about 20 km). 51 samples could be used in this analysis. We found that our wind estimates were biased high by about 2 m/s. The same order of bias was found when inverting by using the CMOD5 [*Hersbach et al.*, 2007] model. So, we conclude that the STORM normalized radar cross-section is probably overestimated, with a bias of about 1.07 dB on the radar cross-section explaining the differences between Pharos and radar winds. Figure 4 shows that after correcting from this bias, a good agreement is found between Pharos winds and radar winds inverted by using CMOD2-I3. The mean bias of wind speed is 0.11 m/s, and the standard deviation is 1.63 m/s.

[34] In the analysis presented in the following sections, the same method is applied to the whole data set: wind direction estimated from the fit of a Fourier series on STORM observations at incidence 32.5°, wind speed estimated from the observations by using the CMOD2-I3 model after correcting from a 1.07 dB bias on the radar cross-section.

4. Results

[35] A total of 164 files have been processed from the raw data of the 15 flights. From this analysis, we obtained the following parameters collocated in space an time: wind speed and wind direction, mean square slope in upwind
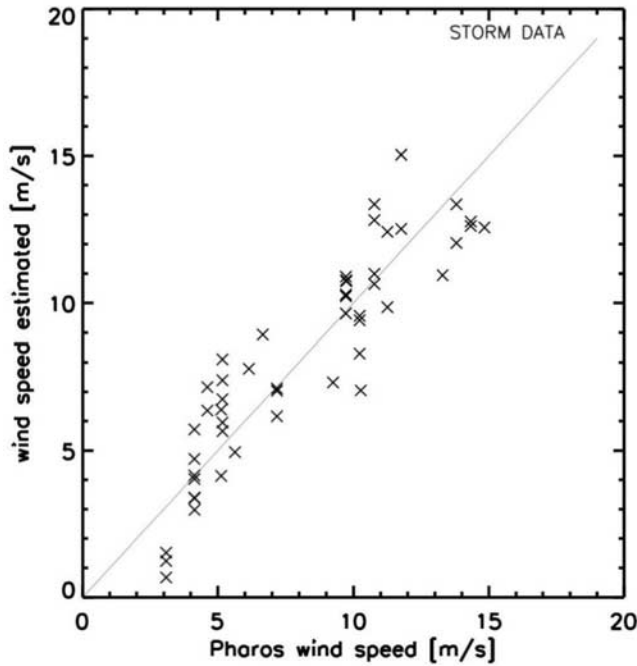
Figure 4. Comparison of wind speed estimated from STORM and wind speed measured at the Pharos buoy. STORM radar cross-sections at incidence 32.5° and corrected from a positive bias of 1.07 dB were used with the CMOD2-I3 to obtain the radar-derived winds.

and crosswind directions, parameters of the non-Gaussian analysis. Each file (i.e., each sample presented in the following) represents observations acquired over 2 to 10 min (variable length), representing a distance of about 12 to 60 km along the flight track.

4.1. Mean Square Slope as a Function of Wind Speed-Gaussian Assumption

[36] As mentioned above, one may consider as a first approximation, that the slope pdf has a Gaussian form. This is what we consider in this section, whereas the non-Gaussian case is discussed in section 4.3.

[37] The mean square slope estimated from the STORM data following the method presented in section 3.1 is plotted in Figure 5 as a function of wind speed. The radar filtered mean square slope increases with wind speed, approximately as a power law of the wind speed rather than a linear dependence as proposed by *Cox and Munk* [1954a, 1954b]. The trend of our results versus wind speed is however close to the logarithmic functional forms proposed by *Wu* [1972] in his reanalysis of the Cox and Munk data (see below and Figures 6b, 6d). This trend is also close to the logarithmic dependence found by *Vandemark et al.* [2004] in his analysis of nadir pointing radar observations in Ka-Band. Furthermore, our results show that the trend is the same in the upwind (Figure 5a) and crosswind (Figure 5b) directions, with however a slightly larger sensitivity to wind speed in the upwind direction (exponent 0.27) than in the crosswind direction (exponent 0.24). The linear relationships proposed by *Cox and Munk* [1954a] are also characterized by a stronger dependence with wind speed in upwind than in crosswind.
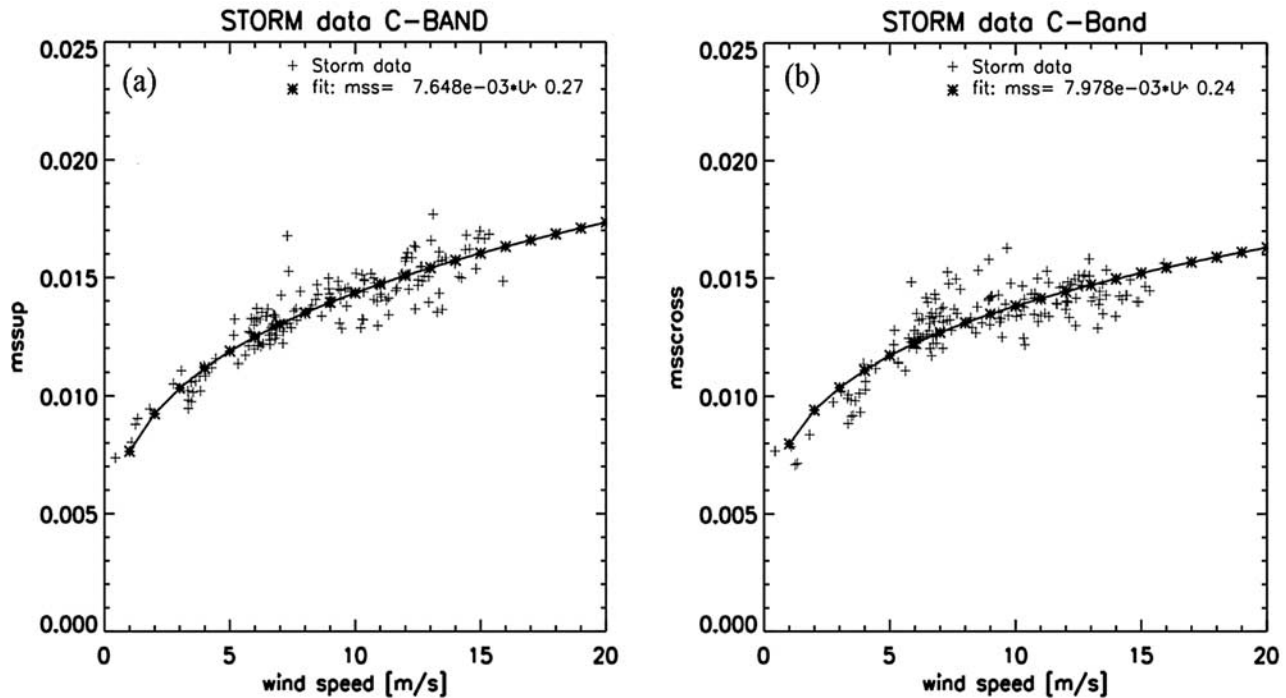

Figure 5. Mean square slope of the waves retrieved from the STORM observations in the incidence range 7−16°, as a function of wind speed estimated from the STORM observations at 32.5° incidence angle. (a) in the upwind direction (b) in the crosswind direction.
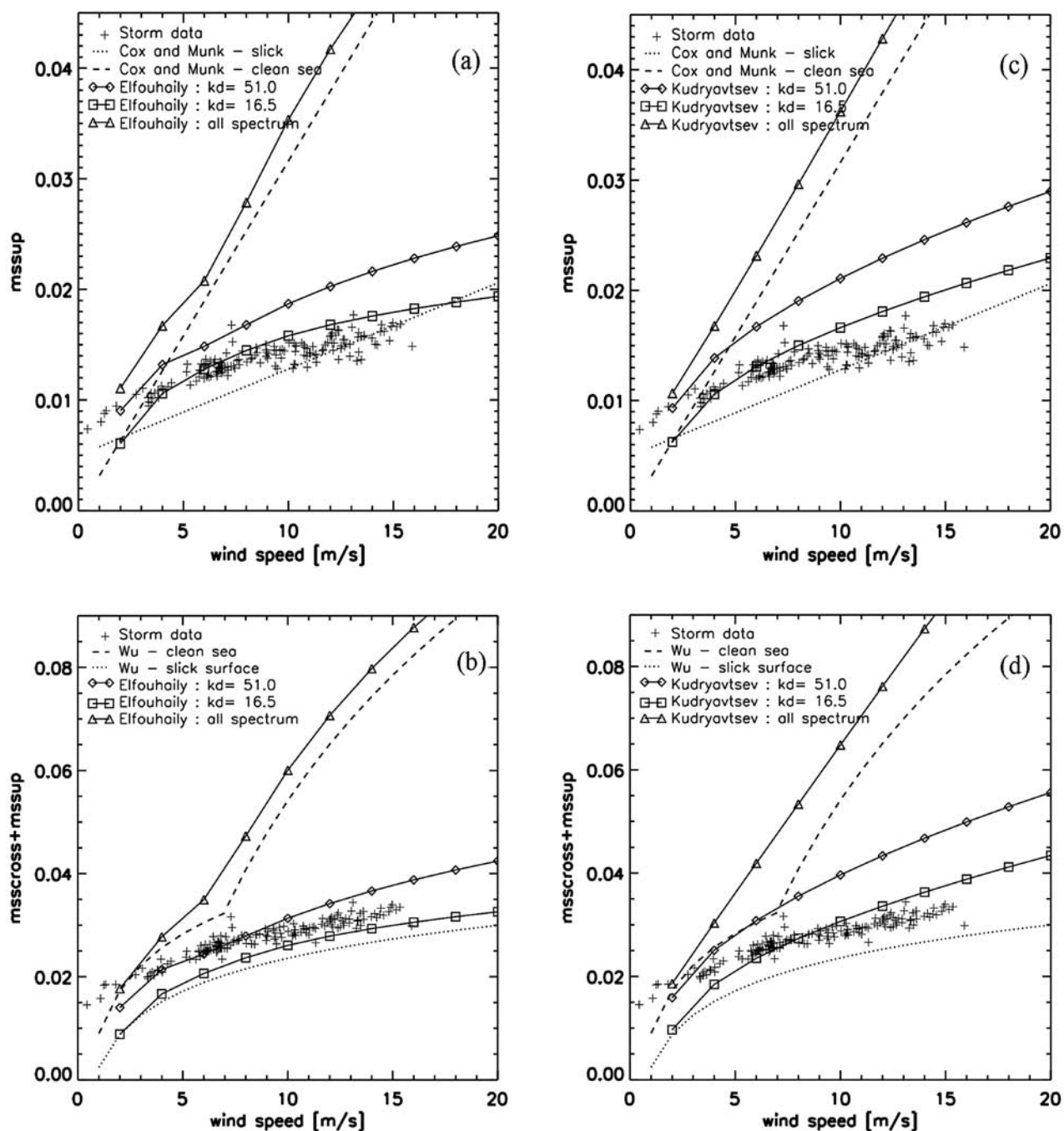
Figure 6. Mean square slope derived from the STORM observations (crosses) versus wind speed in the upwind direction (a) and (c) and as total value (upwind + crosswind) (b) and (d). In Figures 6a and 6b, respectively in Figures 6c and 6d, we compare the radar results with the mss estimated from the ECKV spectrum (respectively from the KHCC spectrum) filtered at $k_d = 51$ rad/m (line with diamonds) or not filtered (line with triangles). The empirical laws given by *Cox and Munk* [1954a] for clean sea (dashed line) and slick sea (dotted line) are also plotted in Figures 6a and 6c. Same in Figures 6b and 6d but for the empirical laws given by *Wu* [1972].

[38] Figures 6a-6d illustrate how these radar derived mean square slopes compare with the relationships given by *Cox and Munk* [1954a, 1954b] or *Wu* [1972] in the case of a clean sea (dashed line) and a sea covered by artificial slick (dotted line). Our radar filtered mss exhibit values intermediate between these two cases for the whole wind speed range. The radar-derived mss corresponds to a "filtered surface", similarly to the case of the slick observations of *Cox and Munk* [1954a] where the shortest waves are damped by the slick. According to the analysis of *Wu*

[1972], the slick case observations of *Cox and Munk* [1954a] correspond to a minimum wavelength of 38 cm (maximum wave number 16.5 rad/m), whereas the implicit filter for the STORM data is of $k_d = 51$ rad/m (see section 3.2). The results shown in Figure 6 are consistent with this, as STORM derived mss are larger than those of the slick case of *Cox and Munk* [1954a, 1954b]. At light wind (<7 m/s) the radar-filtered values are in between the two empirical curves relative to clean sea and slick sea, whereas at higher winds, they are much closer to the slick case than to the clean sea case. This can be related to the fact that the contribution of the short waves (less than 51 rad/m in wave number) to the total mss at light wind is less, in a relative sense, than at strong wind [see also *Jackson et al.*, 1992]. The sensitivity to wind speed is also close to that given by the relation of the slick case, but much weaker than in the case of clean sea.

[39] Figures 6a-6b (resp. Figures 6c-6d) also show the mean square slope calculated from the integration of the ECKV spectrum (resp. KHCC) over different wave number ranges (full range: line with triangles, up to $k_d = 51$ rad/m: line with diamonds, up to $k_d = 16.5$ rad/m: line with squares).

[40] Compared to the mss of the ECKV spectrum filtered at a maximum wave number of 51 rad/m (solid line with diamonds), our results show smaller mss in the upwind direction (up to 35% overestimation of mss from ECKV), but a much better agreement for the total filtered mean square slope (sum of upwind and crosswind), with a maximum overestimate from ECKV spectrum, of about 8% at high winds. The comparison between the slick sea case of Cox and Munk and the mss from the ECKV spectrum filtered at 16.5 rad/m leads to the same conclusion: overestimate of the upwind mss from the ECKV spectrum, good agreement for the total mss. The mss calculated over the whole wave number range of the ECKV spectrum (solid lines with triangles in Figures 6a-6b), shows only a slight overestimate (about 12%) with respect to the clean sea relationship of *Cox and Munk* [1954a, 1954b] both for upwind and total values. All these comparisons indicate that the ECKV spectrum i) provides a total or omni-directional mss in good agreement with values obtained from remote sensing (optics or microwave), which filter scales smaller than 12 cm, ii) shows deficiencies for the directional aspects, with an overestimation of the upwind mss for wavelengths larger than 12 cm (51 rad/m) compensated by a underestimation of the crosswind corresponding mss (not shown). The directional aspects of the mss are further discussed in section 4.2 below.

[41] Figures 6c-6d show the same type of comparisons but with the KHCC spectrum. The radar derived mss are much smaller than those derived from the KHCC spectrum filtered at $k_d = 51$ rad/m, both in the upwind direction and as total values (sum of upwind and crosswind). The same overestimation is also observed in the crosswind direction (not shown). The conclusions are the same for the mss calculated from the KHCC spectrum over the whole wave number range and compared to the clean sea curve of *Cox and Munk* [1954a, 1954b] or for the mss calculated from the KHCC spectrum filtered at 16.5 rad/m compared to the slick curve of *Cox and Munk* [1954a, 1954b]. Hence the KHCC

spectrum gives a too high mean square slope over the whole domain of wavelengths and in all directions.

[42] *Hwang* [2005] presents in situ measurements of surface slopes of short waves. His observations, performed using a free-drifting technique, cover the range 0.02 to 6 m. From these observations, *Hwang* [2005] propose an analytical expression of the wave spectrum for short waves, and estimate the dependence of the mss with the upper bound wave number. To estimate the mss, Hwang however parameterizes the full wave spectrum by summing spectra from two different parameterizations, for wave number smaller and larger than 1 rad/m, respectively, with the spectrum of short waves derived from the measurements of *Hwang and Wang* [2004]. This leads to an unrealistic discontinuity in the spectrum, particularly at high winds, which may affect the total mean square slope. A comparison of our results with his Figure 3 shows that for winds larger than 6 m/s our radar-derived mss slopes are smaller than those shown in Figure 3 of Hwang or given by his analytical formulation equation (5), taking into account a maximum wave number of 51 rad/m. This is probably to be related to the drawback of Hwang's parameterization mentioned above.

[43] *Jackson et al.* [1992] also derived filtered mss from radar observations, but at Ku-Band. Compared with their results we find smaller values. This is expected since the radar wavelength is longer is our case. Taking into account the wave number cutoff associated with our observations (51 rad/m- see section 3.2), our results are quite consistent with the analysis presented by Jackson et al. for different wave number cutoffs (his Figure 14).

4.2. Anisotropy of the Mean Square Slope (Gaussian Assumption)

[44] Figure 7 shows the comparison of the crosswind to upwind ratio of the radar-derived mss. The radar-derived values of the crosswind to upwind ratio range from about 0.8 to 1.15. The mean value is 0.97 and the trend with wind speed is weak. Using the power relationships fitted to the data (lines in Figures 5a-5b), we find that the mean trend of the crosswind to downwind ratio is a slight decrease with wind speed (Figure 7), i.e., a slight increase of the upwind to crosswind ratio with wind speed.

[45] In Figures 8a-8b, the results are compared with the anisotropy of the mss derived from the ECKV and KHCC spectra, and the one given by the *Cox and Munk* [1954a, 1954b] relationship (slick and clean sea).

[46] Compared with the anisotropy found by *Cox and Munk* [1954a, 1954b] (slick sea), the radar derived anisotropy shows the same order of magnitude at moderate winds (>10 m/s), but is smaller at light wind. The crosswind to upwind ratio of the mss derived from the ECKV spectrum filtered at $k_d = 51$ rad/m (line with diamonds in Figure 8a) is smaller (0.6 to 0.7) – i.e., the anisotropy is larger. The same conclusion is reached when we compare the mss derived from the ECKV spectrum filtered at $k_d = 16.5$ rad/m to the slick curve. This indicates that the anisotropy of the ECKV spectrum is not in very good agreement with remote sensing observations (optics or radar).

[47] The anisotropy of the mss derived from the KHCC spectrum filtered at $k_d = 51$ rad/m (line with diamonds in Figure 8b) shows the same order of magnitude as the radar-derived values, at least at moderate winds (>10 m/s), but is
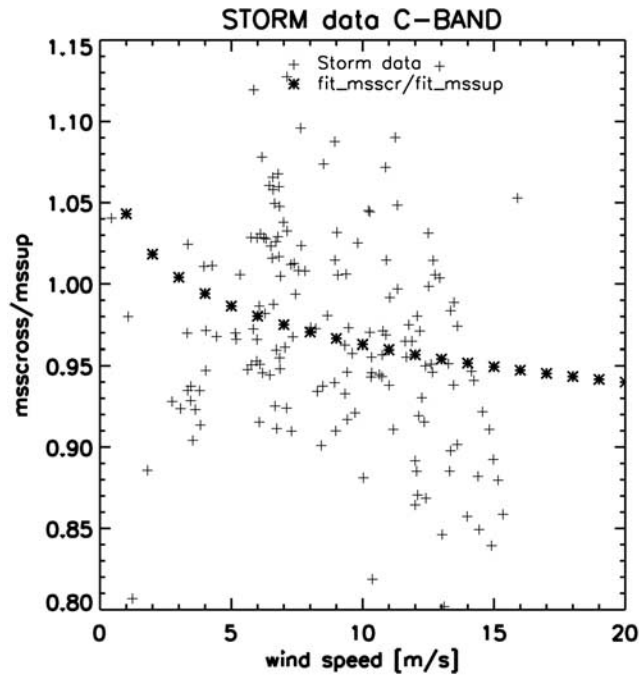
Figure 7. Crosswind to upwind ratio of the mss derived from STORM data, as a function of wind speed. The stars represent the ratio of the power laws fitted in the crosswind and upwind directions, respectively.

larger (smaller value of the ratio) at light wind. When the range of wave number is restricted to $k_d < 16.5$ rad/m, the mss derived from the KHCC model is consistent with the *Cox and Munk* [1954a, 1954b] relationship of the slick case. At least the agreement is much better than when the same comparison is done with the ECKV spectrum.

[48] In summary, we conclude from this set of comparisons that the KHCC spectrum overestimates the radar-derived filtered mss in upwind and crosswind directions (and also the total or omni-directional values; see section 4.1), but that its anisotropy is consistent with the *Cox and Munk* [1954a, 1954b] relationship in the slick case and rather consistent with our radar-derived estimates. In contrast, whereas the ECKV spectrum gives consistent results for the total mss (sum of upwind and crosswind), its anisotropy is much too large compared with our radar-derived results and with the slick case of *Cox and Munk* [1954a].

[49] The role of the different parts of the surface spectrum contributing to this behavior (low frequency waves or waves in the equilibrium domain) is illustrated in Figure 9, which shows the crosswind to upwind ratio of the mss for each component of the spectra and for the total spectra. The expressions used for these different parts of the spectra are recalled in Appendix B, with mss estimated in all cases for wave numbers less than 51 rad/m. Figure 9 shows that in the case of the ECKV spectrum, the underestimate of the crosswind to upwind ratio compared to the radar-derived values (overestimate of the anisotropy) is due to the combination of a significant anisotropy for both the low frequency part and for the equilibrium part (also called ripple part) of the spectrum. Assuming that the anisotropy of the long-wave part is correct (obtained from the observations of
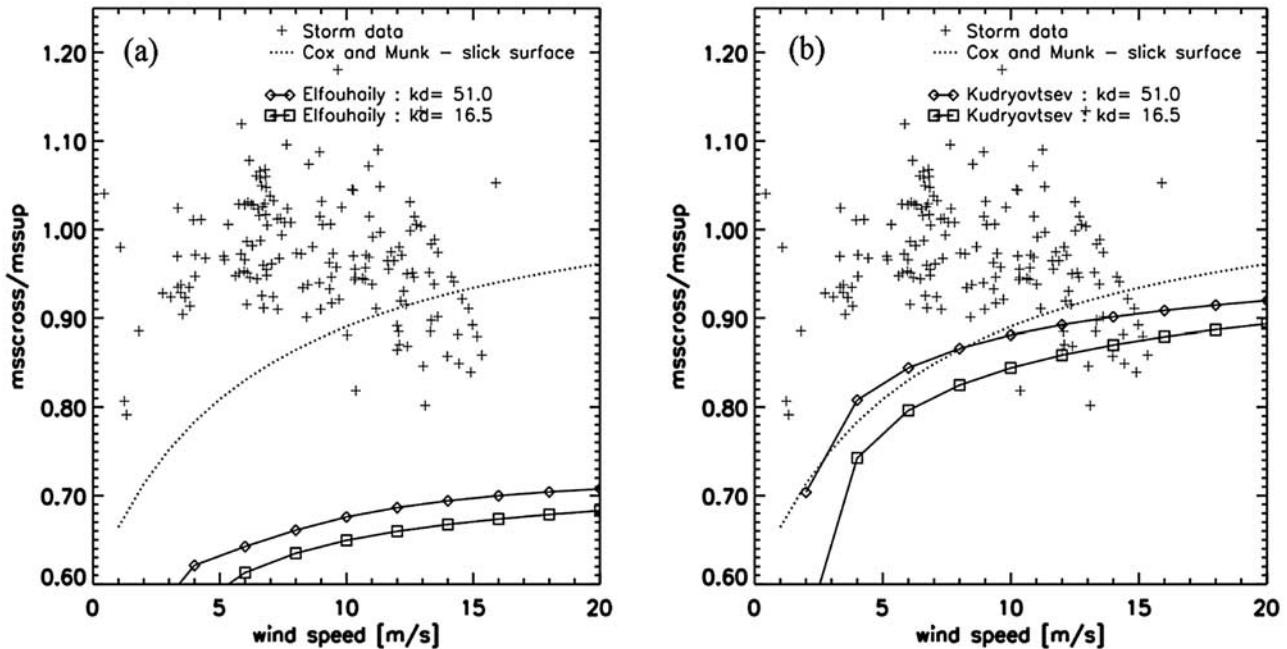

Figure 8. Crosswind to upwind ratio of the mean square slope as derived from the STORM radar observations versus wind speed (cross symbols). The corresponding values deduced from the EKCV (a) and KHCC (b) spectra, filtered at $k_d = 51$ rad/m (diamonds) or $k_d = 16.5$ rad/m (squares) are also plotted. The empirical relationship given by *Cox and Munk* [1954a, 1954b] for the slick case is shown as the dotted line.
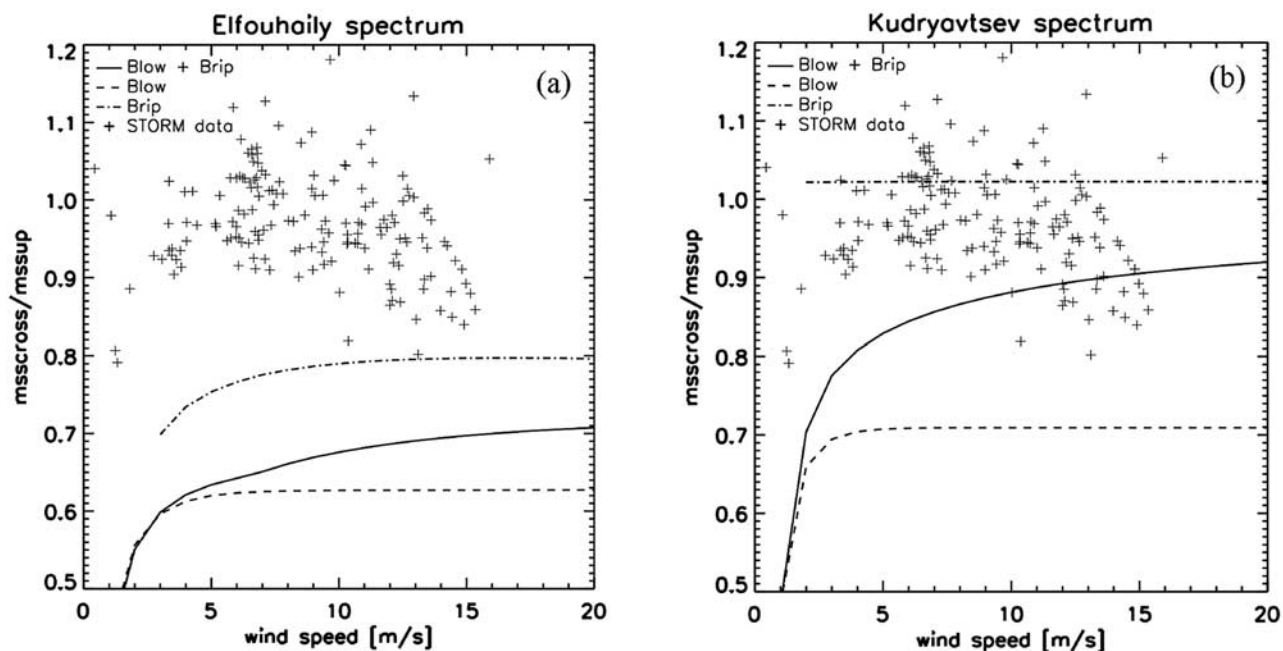
Figure 9. Same as Figure 8, except that the curves represent the crosswind to upwind ratio of mss estimated from the different components of the surface spectrum models: Low frequency part (dashed line), high frequency part limited at $k_d < 51$ rad/m (dashed-dotted), and sum of both parts (solid line). The expressions of the spectra are recalled in Appendix B.

Donelan et al., 1985), we conclude that the equilibrium part of the ECKV spectrum shows a too large anisotropy. Note however that ECKV tuned some coefficients of their angular formulation, so that the mss of the spectrum (full range) agrees with the data of Cox and Munk in the clean sea case. Therefore we conclude that the ECKV spectrum probably exhibits a too small anisotropy of waves with wave numbers larger than 51 rad/m, which compensates the too large anisotropy of the rest of the spectrum. This is indeed what was found by *Mc Daniel* [2001] and *Mouche et al.* [2006] in their analysis of Bragg wave anisotropy (wave numbers around 150–180 rad/m) from radar data at medium incidence (40–50°).

[50] In contrast, the KHCC spectrum corresponds to an anisotropy of the mss in better agreement with radar-derived data. Since the long wave spectrum gives an anisotropy of the same order as that with the long wave part of ECKV spectrum, and can be assumed reliable (known from the observations of *Donelan et al.*, 1985), we conclude that the anisotropy of the equilibrium part of the KHCC spectrum (almost no anisotropy) is compatible with the radar-derived values.

[51] Another remark from this comparison is that the trend of the total mss with wind speed (important decrease of the anisotropy between 1 and 7 m/s) given by either the ECKV spectrum or the KHCC spectrum is due to the decrease of anisotropy of the long waves with wind speed.

[52] In summary, we have shown in this section that:

[53] The radar filtered mss follows a power law function of wind speed (exponent 0.27 in upwind, 0.24 in crosswind), close to the one proposed by *Wu* [1972] in his reanalysis of *Cox and Munk* [1954a, 1954b] data in the case of observations with slick.

[54] The anisotropy of the radar-filtered mss is small and its dependence with wind is weak.

[55] The *Elfouhaily et al.* [1997] spectrum is in good agreement with the radar-derived results when analyzed as omni-directional values, but show deficiencies of its anisotropy description, with a too large anisotropy of intermediate waves (waves within the equilibrium range, but with wave numbers smaller than 51 rad/m).

[56] The *Kudryavtsev et al.* [2003] spectrum provides too large mss in all directions, compared to radar observations, or to *Cox and Munk* [1954a] observations, but the anisotropy of the mss is in rather good agreement with our observations and with those of Cox and Munk for the slick case.

4.3. Non Gaussian Analysis

[57] In this section we analyze the radar observations by extending the approach to a non-Gaussian analysis, as explained in section 3.3.

[58] The peakedness and overall mss parameters have been first derived for each radar sample of the 164 files of the 15 flights. Figure 10 shows two examples of the peakedness parameter and overall mss as a function of azimuth angle for files representing 4 min of data each. Figure 10a corresponds to a high wind speed (14 m/s) whereas Figure 10b corresponds to a low wind speed case (5 m/s). In both cases, there is no clear evidence of an azimuth modulation of the peakedness parameter, which validates a posteriori the assumption used to write equation (10). The scatter of the peakedness value is rather large, particularly in the high wind case (see Figure 10a). It must be noted that in this non-Gaussian analysis, some samples have been rejected when the negative values of peakedness were
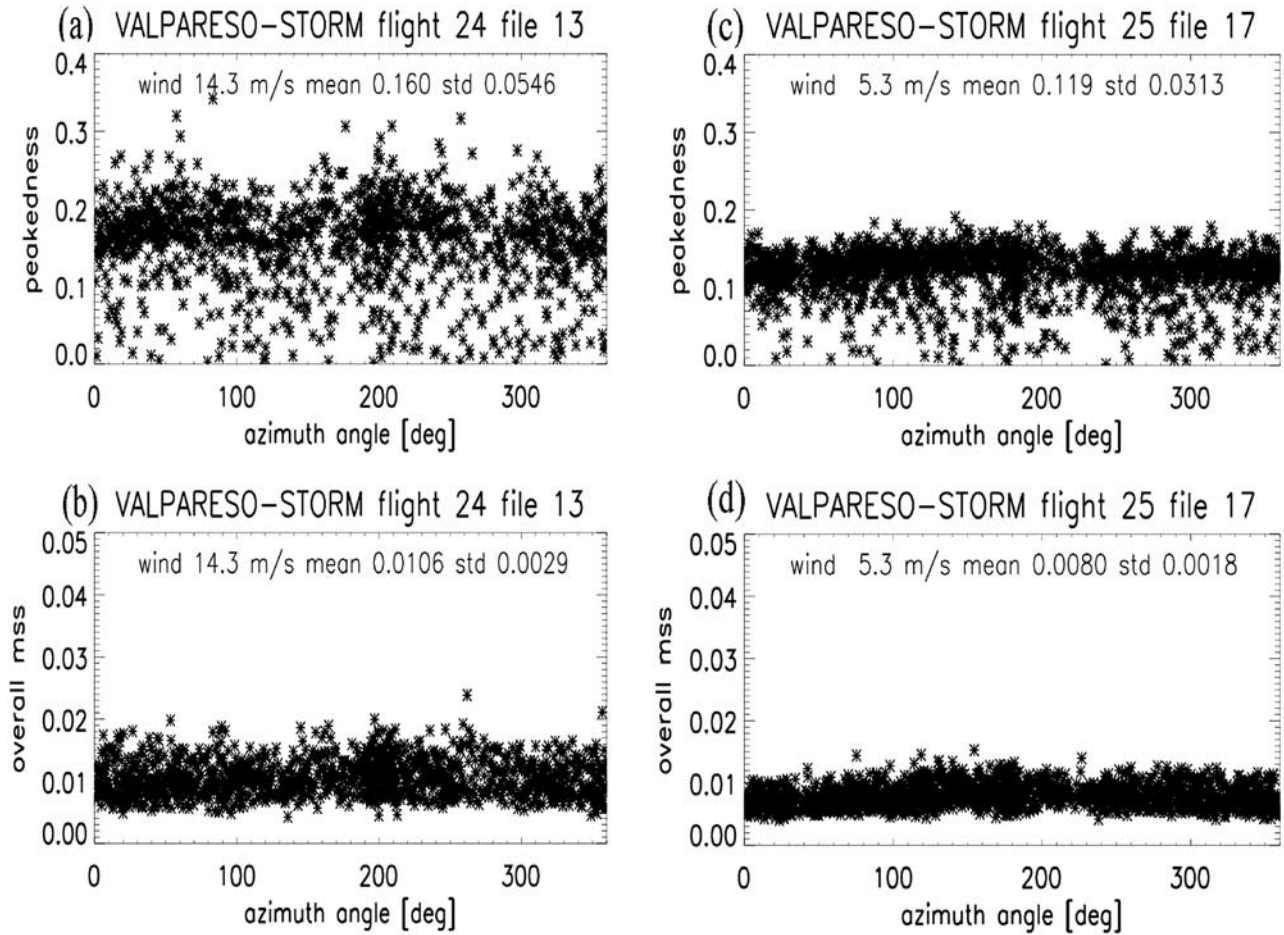
Figure 10. Peakedness (a and c) and overall mss (b and d) deduced from STORM observations as a function of azimuth angle in two different situations: in a strong wind case (14 m/s) in Figures 10a–10b, and a light wind case (4 m/s) in c and d.

obtained (this represents between 5 and 20% of the samples, depending on the conditions).

[59] From this analysis, applied to our 164 files, we derived the mean peakedness and mean overall mss for each file, and analyzed the results versus wind speed estimated from the radar data obtained at the same time and location. The results are illustrated in Figures 11a-11b. We find that the peakedness parameter varies between 0.08 and 0.18, for wind speed increasing from 1 to 16 m/s, but the main increase occurs at wind speed smaller than 7 m/s, whereas the peakedness remains almost constant for winds above this value. By simulating the pdf of the compound
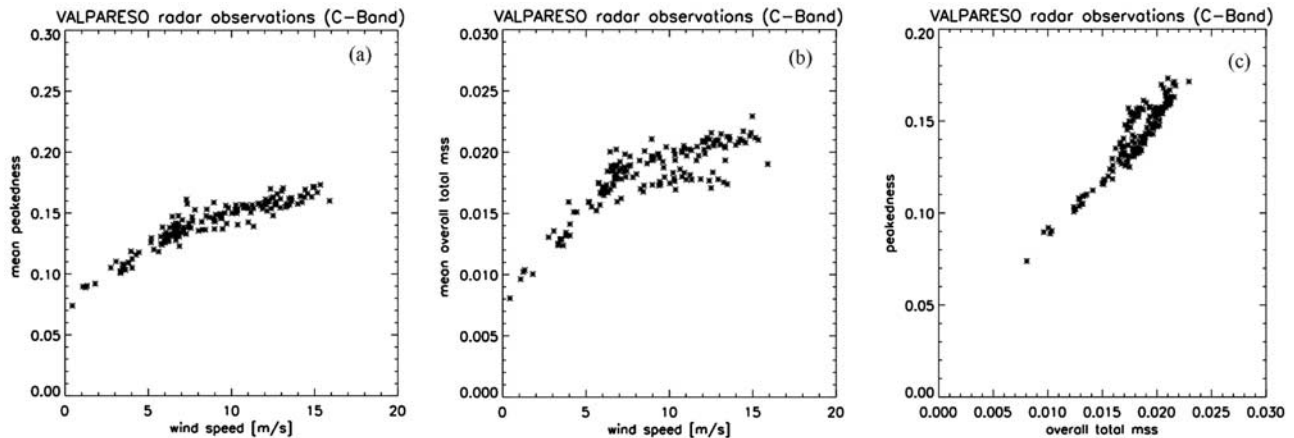

Figure 11. Peakedness parameter (a), and overall mean square slope (b) deduced from the complete set of STORM observations and plotted as a function of wind speed. (c): peakedness parameter as a function of the overall mean square slope, for the same data set.

model (equation (11)), it can be shown that this range of peakedness values (Δ from 0.08 to 0.18) corresponds to a kurtosis excess coefficient of the compound slope pdf between 0.24 and 0.44.

[60] The deviation from Gaussian statistics is very small at light wind (peakedness less than 0.1 or kurtosis excess factor close to 0.25 for wind speed less than 4 m/s), and increases with wind speed with a change in the sensitivity to wind speed around 7 m/s. The overall mean square slope has the same behavior, with a larger increase with wind speed up to 7 m/s and a nearly constant value at wind speed larger than 7 m/s. It is interesting to note that this change occurs at a wind threshold mentioned in several publications as corresponding to changes in the backscatter signatures associated with changes in aerodynamic regime from smooth to rough, and to the onset on intensive breaking events. The similar dependence with wind speed of the peakedness parameter and of the overall mean square slope (see Figures 11a–11b) leads to a very good correlation between these two parameters: a linear dependence with a correlation coefficient 0.94 is found (see Figure 11c). The overall mean square slope (parameter $1/\alpha_0$, see section 3.3), expressed as non-directional total value, follows the same trend with wind speed as in the case of the mss derived in the Gaussian case, but with significantly smaller values (compare Figure 11b with Figure 6d).

[61] There are only very few publications that can be used as references to be compared with our results. As explained in *Chapron et al.* [2000], the correction factor proposed by *Cox and Munk* [1956] to provide total mean square slope from their optical measurements, may be interpreted as an *ad'hoc* correction to account for deviation from Gaussian statistics, with a peakedness factor Δ of 0.20 in the slick case and 0.23 in the clean sea case. The order of magnitude of our STORM derived peakedness values (up to 0.18) is consistent with this. Although Δ is slightly smaller in our case, the difference in terms of excess kurtosis parameter is small (0.44 for $\Delta = 0.18$, 0.46 to 0.47 for $\Delta = 0.20$ to 0.23). *Cox and Munk* [1954a, 1954b] suggest that the peakedness of the slope pdf is constant with wind speed. We find here that the peakedness parameters increases with wind speed, but mainly for winds below 7 m/s. At stronger winds, the peakedness parameter saturates, with a trend similar to that of the effective mss estimated from the Gaussian analysis (see above). *Vandemark et al.* [2004] also analyzed the slope pdf of waves using precise slope measurements from an airborne laser; their results however, concern waves with wavelengths larger than 2 m and their study is restricted to a non-directional analysis. They found larger values for the excess kurtosis parameter (between 1.5 and 3 depending on wind speed), with a minimum value reached at a wind speed of about 10 m/s. *Shaw and Churnside* [1997], from scanning-laser measurements of the surface glint under wind conditions from 4 to 9 m/s, found a kurtosis value between 0.4 and 2.6, only weakly correlated with wind speed (decreasing with wind speed) but more significantly correlated to the instability of the air-sea interface. Correlatively they did not find any significant correlation between kurtosis and mean square slope, whereas our results do show such a correlation (Figure 11c). The order of magnitude of our kurtosis value corresponds to the lowest value estimated by Shaw and Churnside.

[62] The comparison of our results with the study of *Chapron et al.* [2000] seems to indicate that the peakedness parameter is only weakly sensitive to the conditions of observations (electromagnetic wavelength, incidence angle), at least compared to the effective mean square slope derived from radar remote sensing observations. Differences with the kurtosis parameter derived from other techniques (range and slope measurements from laser by *Vandemark et al.* [2004], laser measurements by *Shaw and Churnside* [1997]) remain however to be explained.

[63] It must be mentioned at this point that we also made tests to invert the peakedness parameter with an alternative assumption in the formulation of the "compound" slope pdf: we assumed that the fluctuations of $1 + \delta$ followed a Gaussian distribution rather than a Gamma distribution. However, in this case, equation (13) leads to solve a second-degree equation, which may have either two solutions or no solution. With this hypothesis, we could process only less than 30% of the data. Results restricted to these cases give, for one of the two solutions, mean peakedness values, which are very close to those shown above in Figure 11a. This indicates that it is indeed necessary to consider that the statistics of fluctuations δ have a skewness differing from zero, but that the deviation of the statistics of δ from Gaussian distribution remains small.

[64] In order to further interpret our results, we performed some simulations of slope pdf, assuming Gaussian and compound models. Slope values in the range [-0.5, +0.5] are considered for these simulations. Figure 12 shows a simulation of Gaussian pdf compared to a "compound model" pdf obtained by combining a Gaussian distribution and a model of fluctuations of the inverse of the mss. Both a Gaussian distribution and a Gamma distribution are considered for the perturbation, with the same variance Δ. For the example shown in Figure 12, the overall total mss is assumed to be equal to 0.012 (close to the directional maximum value found here from data analysis), and the Δ parameter is fixed to 0.20 (close to the maximum values found here). Figure 12 confirms that both compound models give very similar results in terms of the slope pdf. Figure 12 also shows that the compound models exhibit an increased probability to observe large slopes with respect to the Gaussian distribution. The variance of the compound model is 14 to 22% larger than the variance of the Gaussian model, for a peakedness parameter between 0.15 and 0.20.

[65] Analyzing the physical processes that explain the non-Gaussian behavior of the wave slope pdf and its variation with wind is out of the scope of this paper. We may however propose some tentative explanation. The variation with wind of the peakedness parameter observed in Figure 11a (increasing rapidly with wind at light wind, but almost constant for winds larger than about 7 m/s) may result from the combined effects of wave-wave interactions and breaking processes: at low wind speed, non-linear wave-wave interactions are sufficiently strong to generate non-Gaussian statistics with increased probability of large slopes, as suggested by *Vandemark et al.* [2004]; deviation from non-Gaussian statistics increases with wind speed (or mean square slope) until wind speed reaches about 7 m/s, when wave breaking starts to counterbalance the impact of these non-linear wave-wave interactions, making the devi-
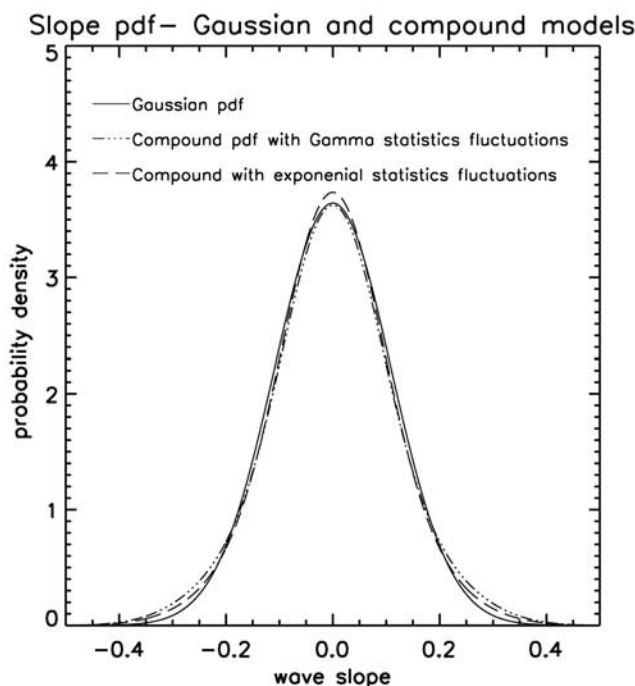
Slope pdf— Gaussian and compound models

Figure 12. Simulation of a compound slope pdf. Solid line: Gaussian pdf with mss 0.012. Dashed-dotted and dashed line: compound model assuming that fluctuations are distributed according to a Gamma (respectively Gaussian) function with a variance 0.20. The resulting pdf has an excess kurtosis parameter of 0.45 in the Gamma case and 0.46 in the Gaussian case. The corresponding mss of the compound pdf is 0.0146 and 0.0132, respectively.

ation from Gaussian statistics virtually constant above about 7 m/s.

5. Conclusions

[66] In this paper we have presented results on the slope pdf estimated from profiles of radar-cross-section at C-band as a function of incidence, for small incidence angles.

[67] We first assessed that in our experimental conditions (C-Band, incidence angles between 7 and 16°) the range of surface waves that affect the radar-derived mean square slope includes waves of scales up to 51 rad/m in wave number. We found that this wave number limit is independent of wind speed when the incidence angle range [7−16°] is used. We confirm that this cut-off limit is however affected by the incidence angle range used in the analysis.

[68] A study of the radar-derived mean square slope as a function of wind was then proposed, using a Gaussian assumption for the slope pdf, and a Geometrical Optics model. One of the originality of this study is that the wind speed was determined for each mss value, perfectly collocated with the mss values, since it was estimated from the same radar data, using moderate incidence angle observations. The trend with wind speed of the upwind, crosswind, and total filtered mss (sum of upwind and crosswind) was presented. Our total mss follows a power law function of wind speed close to the one proposed by *Wu* [1972] in his reanalysis of the slick case data of *Cox and Munk* [1954b].

We found a small anisotropy of the radar-derived mss, with no significant variation with wind speed. The total mss derived from *Elfouhaily et al.* [1997] spectrum filtered at 51 rad/m was found to be in good agreement with our results, but the corresponding mss anisotropy derived from *Elfouhaily et al.* [1997] spectrum is too large compared to our observations. In contrast, the mss anisotropy of *Kudryavtsev et al.* [2003] spectrum is rather consistent with our results, but the total, upwind, and crosswind mss are relatively too large. From an analysis performed by separating the contributions of the short waves and long-wave parts of the model spectrum, we conclude that in the case of Elfouhaily et al. spectrum, the overestimate of the mss anisotropy is due to the intermediate waves within the equilibrium range but with wave numbers smaller than 51 rad/m. This confirms the results of *Mc Daniel* [2001] who found, from a comparison of observations with simulations with a small-slope approximation model, that the Elfouhaily et al. spectrum is too anisotropic to provide an upwind to crosswind ratio of the radar signal, consistent with C and Ku-band observations at incidence smaller than 25°, but that this spectrum is also too isotropic in the Bragg regime (see Figure 10 of Mc Daniel). We also show that improvements of the Kudryavtsev et al. spectrum should be proposed to reproduce the upwind and crosswind mss better, without changing the anisotropy very much.

[69] A further analysis was proposed in the present paper, by using a non-Gaussian hypothesis, based on the compound model proposed by *Chapron et al.* [2000]. This compound model is equivalent to assuming a non-Gaussian shape of the slope pdf, with a kurtosis related to a so-called peakedness parameter Δ, which characterizes the variance of a mean square slope distribution estimated over the surface sampled by radar. To our knowledge, it is the first time that peakedness values are explicitly derived from radar observations, and documented as a function of azimuth and wind speed. Our results show that the slope pdf that leads to the best fit of the radar cross-section profile with incidence, exhibits a positive excess kurtosis leading to a higher probability of observing large slopes. We find that the peakedness factor (expressed as in the model of *Chapron et al.*, 2000) ranges between 0.11 and 0.18 with the higher values (0.18) encountered at winds above 7 m/s. This corresponds to an excess kurtosis parameter of the order of 0.45. The peakedness factor increases significantly between 1 and 7 m/s and then remains almost constant. No variation of the peakedness factor with azimuth is evidenced. Another result of our study is that our radar data set could be analyzed with the compound model proposed by *Chapron et al.* [2000] only if a Gamma distribution for the fluctuations of the local mss was assumed. With a Gaussian distribution for these fluctuations, the majority of radar samples cannot be inverted. This indicates that a Gamma distribution should be preferred in the compound model proposed by *Chapron et al.* [2000]. The modeling study proposed by *Bourlier* [2004], which takes into account non Gaussian statistics of the surface, is also qualitatively consistent with our results: kurtosis impacts the dependence of the radar cross-section with incidence at small incidence. Further work should be carried out to compare in a quantitative way, observations and model results obtained under a non-Gaussian assumption.

[70] All these results on the non-Gaussian behavior of the slope pdf are important and should therefore be studied further. The non-Gaussian behavior affects the modeling and interpretation of altimeter data. It may also influence the absolute calibration of the radar cross-section of radar altimeters [*Caudal et al.*, 2005]. It is important to be assessed for the modeling of bi-static backscatter coefficients (for modeling or inverting GPS signal in particular; see *Thompson et al.*, 2005). It is linked to the hydrodynamics of the surface (non-linear interactions, breaking,...), so that a better documentation of the non-Gaussian behavior of the surface will help to understand and model these hydrodynamic processes better.

[71] This study has also shown the value of observing the ocean surface by using a multiple incidence geometry. In the future, data from the TRMM radar could be used to extend this study to Ku-Band observations, in particular to check that the estimated kurtosis (or peakedness) does not depend on the radar wavelength. It would also permit a more extensive investigation of the behavior of peakedness with wind speed. The approach proposed here however, is not appropriate for estimating another important parameter of the non Gaussian distribution, namely the skewness of the pdf of surface heights. Other methods should be developed to estimate this quantity from remote sensing observations.

Appendix A: Physical Optics Model

[72] Several authors give the general expressions for the Physical Optics (see e.g., the review by *Elfouhaily and Guérin*, 2004). In the present case, where we deal with backscattering conditions, the expressions given by *Mouche et al.* [2007] for the normalized radar cross-section σ_0 can be considered. They are based on the assumption that the statistics of sea surface height follow a Gaussian law:

$$\sigma_0 = \left| \frac{K(\mathbf{k}, \mathbf{k_0})}{Q_z} \right|^2 \int_{\mathbf{r}} e^{-Q_z^2[\rho(0-\rho(\mathbf{r}))]} e^{-i\mathbf{Q_H} \cdot \mathbf{r}} d\mathbf{r} \qquad (A1)$$

where $\rho(\mathbf{r})$ is the correlation function of the sea surface height at a given length $\mathbf{r}$, $\mathbf{k_0}$ and $\mathbf{k}$ are the horizontal projections of the incident and scattered wave numbers, respectively, Q_z and $\mathbf{Q_H}$ are the vertical and horizontal components of the momentum transfer vector $\mathbf{Q}$, which is the difference between backscattered and incident wave number vectors. In the case considered here of backscattering conditions, $Q_z = 2k_0\cos\theta$, and $\mathbf{Q_H} = 2\mathbf{k_0}\sin\theta$, where θ is the incidence angle with respect to nadir. $K(\mathbf{k}, \mathbf{k_0})$ is the so-called Kirchhoff kernel, calculated in the fully dielectric conditions, as given by *Elfouhaily et al.* [2003].

[73] In the present study, equation (A1) has been implemented to calculate the backscatter cross-section in C-Band and for small incidence angles (0-20°). Expression for the Kirchhoff kernel was taken from *Elfouhaily et al.* [2003] in the fully dielectric case. The correlation function $\rho(\vec{r})$ was calculated, using a prescribed 2D wave spectrum (either the *Kudryavtsev et al.* [2003] spectrum or the *Elfouhaily et al.* [1997] spectrum).

[74] It is worthwhile to note that when it can be assumed that the microwave wavelength is much smaller than the radius of curvature of the scattering surface, expression (A1) reduces to the GO model [see also *Elfouhaily and Guérin*, 2004 or *Thompson et al.*, 2005]. Indeed, in this case curvature effects and diffraction effects associated to small scales can be neglected, and the correlation function can be expressed as a Taylor expansion about zero up to the second order. Hence with a Gaussian slope statistics, the analytical evaluation of the Kirchhoff integral (A1) yields to equation (2), with $|R|^2 = |k_{0z}^2 K(\mathbf{k}, \mathbf{k_0})/k_0^2|^2$ where $\mathbf{k_{0z}}$ is the vertical component of the backscattered wave number.

Appendix B: Surface Wave Spectra

[75] For the simulations of radar-cross-sections discussed in section 3.2, a surface correlation function must be prescribed in the Physical Optics model (see also Appendix A above).

[76] We choose two different wave spectra. The first one (KHCC) follows the model of *Kudryavtsev et al.* [1999, 2003], the second one (ECKV), the model of *Elfouhaily et al.* [1997]. In both cases, a low-wave number part S_l, and a high-wave number part S_h are defined and combined to obtain a total spectrum.

[77] The KHCC total wave height directional spectrum, $S_K(k, \varphi)$, is:

$$S_K(k,\varphi) = S_{lK}(k,\varphi) \exp(h(k)) + S_{hK}(k,\varphi)(1 - \exp(h(k)))$$

$$(B1)$$

where k is the wave number, φ the direction of propagation. In (B1), $S_l(k, \varphi)$ follows the parameterization of *Donelan et al.* [1985], and the high wave number part, S_{hK}, has been established by *Kudryavtsev et al.* [1999, 2003] using physical considerations on wave growth and dissipation. In (B1), the exponential terms are used to cutoff the contributions of both $S_{lK}(k, \varphi)$ at large wave numbers and of $S_{hK}(k, \varphi)$ at low wave numbers. The expression of $h(k)$ follows the cutoff term used by *Elfouhaily et al.* [1997] to limit the energy of the long waves for wave number larger than $10k_p$, where k_p is the wave number at the peak of the spectrum:

$$h(k) = -\frac{\Omega}{\sqrt{10}} \left(\sqrt{\frac{k}{k_p}} - 1 \right) \qquad (B2)$$

where Ω is the inverse wave age parameter.

[78] $S_{hK}(k, \varphi)$ follows the expression proposed by *Kudryavtsev et al.* [2003], which is recalled here below, neglecting the contribution of the capillary waves, which do not contribute to radar response in C-Band:

$$S_{hK}(k,\varphi)k^4 = B_{hK}(k,\varphi) = \alpha[(\beta_\nu(k,\varphi))]^{1/n} \qquad (B3)$$

with

$$\beta_\nu(k,\varphi) = \left(C_\beta \frac{u_*^2}{c^2} - \frac{4\nu k^2}{\omega} \right) \exp\left[-(\varphi - \varphi_w)^2 \right] \qquad (B4)$$

where $\beta_\nu(k)$ is the effective growth rate, C_β is a growth rate parameter, u_* the air friction velocity, c the phase velocity, ν

the viscosity coefficient, φ_w the wind direction. The dispersion relation links the frequency ω and the wave number k. Parameters C_β, n and α in (B3) have been fixed as in *Kudryavtsev et al.* [2003].

[79] The total ECKV wave height spectrum, combining low and high frequency parts is given by:

$$S_E(k, \phi) = \frac{1}{2\pi} k^{-4} [B_{lE}(k) + B_{hE}(k)][1 + \Delta(k) \cos(2(\varphi - \varphi_w))]$$

$$(B5)$$

where $B_{lE}(k)$ and $B_{hE}(k)$ are the curvature omni-directional spectra of the long and short waves, respectively, and $\Delta(k)$ is the spreading function proposed by *Elfouhaily et al.* [1997].

[80] The expressions of $B_{lE}(k)$ and $B_{hE}(k)$ are those given by *Elfouhaily et al.* [1997] for infinite fetch. Note that, as defined by *Elfouhaily et al.* [1997], the expression of $B_{lE}(k)$ is close to the parameterization of *Donelan et al.* [1985], with however an additional cut-off term, expressed as $\exp(h(k))$, with $h(k)$ given by (B2), included to limit the contribution of long waves for wave number values larger than the peak of the spectrum ($k > 10k_p$).

References

Barrick, D. E. (1968a), Relationship between slope probability density function and the physical optics integral in rough surface scattering, *Proc. IEEE*, 56(18), 1728–1729.

Barrick, D. E. (1968b), Rough surface scattering based on the specular point theory, *IEEE. Trans. Antennas Propag.*, AP-16, 449–454.

Bentamy, A., Y. Quilfen, P. Queffeulou, and A. Cavanie (1994), Calibration of the ERS-1 scatterometer C-band model, *Tech. Rep. DRO/OS-94-01*, 72 pp., Inst. Fr. Rech. Pour l'Exploit. de la Mer, Brest, France.

Bourlier, C. (2004), Azimuthal harmonic coefficients of the microwave backscattering from a non-Gaussian ocean surface with the first-order SSA model, *IEEE Trans. Geosci. Remote Sens.*, 42(11), 2600–2611.

Caudal, G. (1993), Self-consistency between wind stress, wave spectrum, and wind-induced wave growth for fully rough air-sea interface, *J. Geophys. Res.*, 98(C12), 22,743–22,752.

Caudal, G., E. Dinnat, and J. Boutin (2005), Absolute calibration of radar altimeters: Consistency with electromagnetic modeling, *J. Atmos. Oceanic Technol.*, 22, 771–781.

Chapron, B., V. Kerbaol, D. Vandemark, and T. Elfouhaily (2000), Importance of peakedness in sea surface slope measurements and applications, *J. Geophys. Res.*, 105(C7), 17,195–17,202.

Chelton, D. B., J. C. Ries, B. J. Haines, L.-L. Fu, P. S. Callahan (2001), Satellite Altimetry, in *Satellite Altimetry and Earth Sciences*, edited by L.-L. Fu and A. Cazenave, Academic Press, 463 pp.

Cox, C., and W. Munk (1954a), Measurement of the roughness of the sea surface from photographs of the sun's glitter, *J. Opt. Soc. Am.*, 44(11), 838–850.

Cox, C., and W. Munk (1954b), Statistics of the sea surface derived from sun glitter, *J. Mar. Res.*, 13, 198–227.

Cox, C., and W. Munk (1956), Slopes of the Sea Surface Deduced From Photographs of Sun Glitter, *Univ. of Calif. Press*, Berkeley.

Donelan, M. A., J. Hamilton, and W. H. Hui (1985), Directional spectra of wind-generated waves, *Phil. Trans. R. Soc. Lond.*, A315, 509–562.

Elfouhaily, T., and C.-A. Guérin (2004), A critical survey of approximate scattering wave theories from random rough surfaces, *Waves in Random Media*, 14(4), 1–40.

Elfouhaily, T., B. Chapron, K. Katsaros, and D. Vandemark (1997), A unified directional spectrum for long and short wind-driven waves, *J. Geophys. Res.*, 102(C7), 15,781–15,796.

Elfouhaily, T., S. Guignard, R. Awadallah, and D. R. Thompson (2003), Local and non-local curvature approximation: A new asymptotic theory for wave scattering, *Waves in Random Media*, 13, 321–337.

Freilich, M. H., and P. G. Challenor (1994), A new approach for determining fully empirical altimeter wind speed model functions, *J. Geophys. Rev.*, 99, 25,051–25,062.

Freilich, M. H., and B. A. Vanhoff (2003), The relationship between winds, surface roughness and radar backscatter at low incidence angles from TRMM precipitation radar measurements, *J. Atmos. Oceanic Technol.*, 20,549–20,562.

Hersbach, H., A. Stoffelen, and S. de Haan (2007), An improved C-Band scatterometer ocean geophysical model function: CMOD5, *J. Geophys. Res.*, 112, C03006, doi:10.1029/2006JC003743.

Hesany, V., W. J. Plant, and W. C. Keller (2000), The normalized radar cross section of the sea at 10° incidence, *IEEE Trans. Geosci. Remote Sens.*, 38(1), 64.

Hwang, P. A. (2005), Wave number spectrum and mean square slope of intermediate-scale ocean surface waves, *J. Geophys. Res.*, 110, C10029, doi:10.1029/2005JC003002.

Hwang, P. A., and D. W. Wang (2004), An empirical investigation of source term balance of small scale surface waves, *Geophys. Res. Lett.*, 31, L15301, doi:10.1029/2004GL020080.

Jackson, F. C., W. T. Walton, and C. Y. Peng (1985), A comparison of in situ and airborne radar observations of ocean wave directionality, *J. Geophys. Res.*, 90(C1), 1005–1018.

Jackson, F. C., W. T. Walton, D. E. Hines, B. A. Walter, and C. Y. Peng (1992), Sea surface mean square slope from Ku-band backscatter data, *J. Geophys. Res.*, 97(C7), 11,411–11,427.

Kudryavtsev, V. N., V. K. Makin, and B. Chapron (1999), Coupled sea surface-atmosphere model. Part 2: Spectrum of short wind waves, *J. Geophys. Res.*, 104(C4), 7625–7639.

Kudryavtsev, V., D. Hauser, G. Caudal, and B. Chapron (2003), A semi-empirical model of the normalized radar cross-section of the sea surface, Part I: The background model, *J. Geophys.*, 108(C3), 10.1029/2001JC001003.

Longuet-Higgins, M. S. (1963), The effects of non-linearities on the statistical distribution in the theory of sea waves, *J. Fluid Mech.*, 17, 459–480.

Longuet-Higgins, M. S. (1982), On the skewness of the sea-surface slopes, *J. Phys. Oceanogr.*, 12, 1283–1291.

Mc Daniel, S. (2001), Small-slope predictions of microwave backscatter from the sea surface, *Waves in Random Media*, 11, 343–360.

Mouche, A. A., D. Hauser, J.-F. Daloze, and C. Guérin (2005), Dual-polarisation measurements at C-Band over the ocean: Results from airborne radar observations and comparison with ENVISAT ASAR data, *IEEE Trans. Geosci. Remote Sens.*, 43(4), 753–769.

Mouche, A. A., D. Hauser, and V. Kudryavtsev (2006), Radar scattering of the ocean surface and sea-surface roughness properties: A combined analysis from dual-polarizations airborne radar observations and models in C-Band, *J. Geophys. Res.*, 111, C09004, doi:10.1029/2005JC003166.

Mouche, A. A., B. Chapron, and N. Reul (2007), A simplified asymptotic theory for ocean surface electromagnetic wave scattering, *Waves in Random and Complex Media*, 17, 321–341, doi:10.1080/17455030701230261.

Shaw, J. A., and J. H. Churnside (1997), Scanning-laser glint measurements of sea-surface slope statistics, *Appl. Opt.*, 36(18), 4202–4213.

Thompson, D. R., T. M. Elfouhaily, and J. L. Garrison (2005), An improved geometrical optics model for bistatic GPS scattering from the ocean surface, *IEEE Trans. Geosci. Remote Sens.*, 43(12), 2810–2821, doi:10.1109/TGRS.2005.857895.

Vandemark, D., B. Chapron, J. Sun, G. H. Crescenti, and H. C. Graber (2004), Ocean wave slope observations using radar backscatter and laser altimeters, *J. Phys. Oceanogr.*, 34, 2825–2842.

Witter, D. L., and D. B. Chelton (1991), A GEOSAT wind speed algorithm and a method for wind-speed algorithm development, *J. Geophys. Res.*, 96, 8853–8860.

Wu, J. (1972), Sea-surface slope and equilibrium wind-wave spectra, *Phys. Fluids*, 15(5), 741–747.

_____

G. Caudal and D. Hauser, CETP-IPSL, CNRS/Université de Versailles St Quentin, 10-12 Avenue de l'Europe, Vélizy 78140, France. (hauser@cetp.ipsl.fr)

S. Guimbard and A. A. Mouche, IFREMER, Brest, France.